Corrosion Science 111 (2016) 822–834

Contents lists available at ScienceDirect

Corrosion Science

journal homepage: www.elsevier.com/locate/corsci

Mechanism of magnetite formation in high temperature corrosion by model naphthenic acids

Peng Jin*, Winston Robbins, Gheorghe Bota

Institute for Corrosion and Multiphase Technology, Ohio University 342 West State Street, Athens, OH, 45701, USA

ARTICLE INFO

Article history:
Received 8 April 2016
Received in revised form 15 June 2016
Accepted 16 June 2016
Available online 17 June 2016

Keywords:
A. Carbon steel
B. SEM
B. TEM
C. Acid corrosion
C. High temperature corrosion

ABSTRACT

Naphthenic acid (NAP) corrosion is a major concern for refineries. The complexity of NAP in crude oil and the sulfidation process hinder a fundamental knowledge of their corrosive behavior. Studies with model acids were performed to explore the corrosion mechanism and magnetite scales were found on carbon steel. Scanning Electron Microscopy (SEM), Transmission Electron Microscopy (TEM), and X-ray diffraction methods detected differences in the quantity and quality of magnetite formed by model acids. These scales exhibited different resistance to higher severity NAP corrosion in a flow through apparatus. Magnetite is proposed to be formed by thermal decomposition of iron naphthenates.

1. Introduction

"Opportunity crudes" with price discounts often come with higher concentrations of corrosive naphthenic acids (NAP) that may force refineries to employ costly strategies, such as alloy upgrades or inhibitor addition. Therefore, there is a strong incentive to study the fundamentals of NAP corrosion [1–5]. NAP refers to the natural carboxylic acids in petroleum typically measured as total acid number (TAN, the amount of potassium hydroxide in mg to neutralize one gram of oil). In the refinery, NAP corrosion is accompanied by corrosion from reactive sulfur compounds so that high-temperature corrosion of steel is commonly represented by three reactions, Eqs. (1)–(3) [6]:

$$Fe + 2RCOOH \rightarrow Fe(RCOO)_2 + H_2 \quad (1)$$

$$Fe + H_2S \rightarrow FeS + H_2 \quad (2)$$

$$Fe(RCOO)_2 + H_2S \rightleftarrows FeS \downarrow + 2RCOOH \quad (3)$$

As generally stated, NAP (RCOOH) reacts to form oil soluble iron naphthenate [$Fe(RCOO)_2$] (Eq. (1)). Because they may decompose to hydrogen sulfide (H_2S), reactive sulfur compounds are typically shown as the reaction of hydrogen sulfide in Eq. (2) (sulfidation). The corrosion product, iron sulfide (FeS), is not oil soluble and grows as a scale on the steel surface. The reaction between the hydrogen sulfide and iron naphthenate is commonly written as equilibrium; however, kinetically, the precipitation of iron sulfide is much faster than the reverse reaction so that soluble iron naphthenate reacts with hydrogen sulfide in solution (Eq. (3)). It is generally accepted that the iron sulfide scale is somewhat protective acting as a permeation barrier, but conditions that contribute to its formation and stability are not well understood [2–8,58].

Although corrosion generally increases with TAN, no strong correlations exist between the concentration of NAP and the corrosion as measured by weight of iron lost from specimens in laboratory experiments. The lack of correlation is often attributed to interactions between NAP and sulfidation process or to differences in structural shape or molecular weight among NAP of different sources [9–13]. No correlation improvement was observed when methods that measured yield of the hydrogen or soluble iron (i.e. iron naphthenates) were used to detect NAP corrosion of iron powder [14,15]. One of the limitations of the iron powder experiment was the precipitation of iron sulfide from the reaction of iron naphthenate with hydrogen sulfide (Eq. (3)). Furthermore, when applied to model fatty acids hydrogen evolution increased with temperature, but above a threshold temperature carbon dioxide (CO_2) was detected in the gas phase [16]. This was attributed to thermal decomposition of iron carboxylates to ketones and insoluble iron oxide (Eqs. (4) & (5)) which began at 250° C, considerably below the 350° C for thermal degradation of acids alone (Eqs. (6) & (7)) [16,17]:

$$Fe(RCOO)_2 \rightarrow FeO + CO_2 + RCOR \quad (4)$$

* Corresponding author.
E-mail addresses: pj221108@ohio.edu, jinp04@gmail.com (P. Jin).

http://dx.doi.org/10.1016/j.corsci.2016.06.019
0010-938X/

$$4FeO \rightarrow Fe_3O_4 + \alpha\text{-}Fe \quad (5)$$

$$RCOOH \rightarrow R\text{-}H + CO_2 \quad (6)$$

$$2RCOOH \rightarrow R\text{-}R + H_2O + CO_2 + CO \quad (7)$$

Eq. (4) shows the thermal decarboxylation of iron carboxylates ($Fe(RCOO)_2$) to ketones (RCOR) and wüstite (FeO) by ketonization [18–21]. Wüstite (FeO) generated in Eq. (4) is not stable and disproportionates to magnetite (Fe_3O_4) (Eq. (5)) [22–27].

The observation that corrosion resistance occurs when a protective scale of magnetite is formed under a sulfide layer has spurred interest in these secondary reactions [28–30]. Separate patents have been issued for the analyses of ketones or magnetite as methods for evaluating the corrosivity of petroleum process streams in laboratory experiments [31,32]. In prior publications, we have described the development of a protocol that evaluates the corrosion resistance of specimen pretreated with an oil when further corrode with commercial NAP at TAN 3.5 in white oil at 343° C [28,33,34]. This protocol has been applied to evaluate a variety of real crude fractions and model solutions [35]. However, the conditions responsible for the formation of magnetite are not well understood. Specifically, could the magnetite scale be formed during corrosion in the absence of a sulfide scale? Consequently, three model acids in sulfur free mineral oil have been tested in the protocol.

The three model acids (4-phenyl butyric acid [PBA], 4-cyclohexyl pentanoic acid [CxPA], and 1-naphthoic acid [NA]) were selected on the basis of availability, boiling point, and structure. PBA and CxPA have a ring remote from a carboxylic group (COOH) [36,37]. The literature reports naphthenic acids consist of mixtures of multi-ring compounds with the CH_2COOH functionality found in aerobic bio-degradation [38,39]. On the other hand, NA has its COOH directly on an aromatic ring and is proposed to represent anaerobic sourced acids [40,41]. Although magnetite on the steel containing 5%wt chromium (5Cr) was reported previously for petroleum fractions or acid mixture, similar observations have not been made on carbon steel alone [29,30]. Here we evaluate the differences among model acids in forming magnetite during corrosion of carbon steel.

2. Experimental

2.1. Experimental materials

One of commonly utilized steels in refineries was selected for experimentation, i.e., the A106 carbon steel (CS). Its chemical composition is shown in Table 1. Steel specimens were machined in the shape of rings with inner diameter 70.43 mm, outer diameter 81.76 mm, and thickness 5 mm. Before experiments, each ring was abraded with 400 and 600-grit silicon-carbide (SiC) paper in succession. Rings were abraded under the flow of isopropanol to prevent oxidation and overheating. After abrading, rings were wiped with a paper towel, rinsed with toluene and acetone, and dried with nitrogen flow. Weights of freshly abraded rings were taken with an analytical balance with the accuracy up to 0.1 mg. Three CS rings were used in the experiment – two for weight loss measurement and one for microscopic analysis. After the experiment, two rings for weight loss measurement were rinsed with toluene and acetone, exposed to the Clarke solution to remove the surface corrosion product scale [42,43], and reweighed. The corrosion rate was calculated according to the weight loss before and after the experiment. The ring for microscopic analysis was preserved in clean mineral oil to prevent degradation of the corrosion product and was rinsed with toluene and acetone just before the microscopic analysis.

2.2. Experimental solutions

Each model acid (PBA, CxPA, or NA) was dissolved in a high boiling white mineral oil to prepare the pretreatment solutions used to pretreat steel rings (Table 2) [30]. All pretreatment solutions were prepared at TAN 1.75. A mixture of NAP obtained from TCI Americas (TCI) was dissolved in the mineral oil to prepare the corrosive solution (TAN 3.5) which was used to attack the scale formed in the pretreatment [30].

2.3. Experimental equipment

The experimental protocol used two different experimental setups:

Rings were pretreated in a closed stirred autoclave with one of the pretreatment solutions at high temperature. The pretreatment solution was stirred continuously while rings were stagnant. The exploded view of the autoclave is shown in Fig. 1.

The scale protectiveness against NAP corrosion under high temperature and high velocity conditions was investigated in a flow-through rotating cylinder autoclave, called the High Velocity Rig (HVR). Rings were mounted in the HVR reactor and rotated at 2000 rpm while the corrosive TAN 3.5 solution flowed over them. This simulates the high flow rate in transfer lines of refineries. The HVR reactor and the scheme of HVR are shown in Fig. 2.

2.4. Experimental procedures

Experimental procedures comprise of two steps – the pretreatment and the challenge as described below.

In the pretreatment, rings were fully immersed in 0.7 l pretreatment solution and the headspace of autoclave was purged with nitrogen gas to remove air/oxygen. The pretreatment started when the temperature was raised to 316 °C and lasted for 24 h. Rings were stagnant in the autoclave and the impeller was rotating at 500 rpm. In the end of the pretreatment, the autoclave was cooled down and the pretreatment solution was drained from rings which were used for weight loss and microscopic analysis.

Under the same conditions another parallel pretreatment was run. In order to assess the protectiveness of scale formed in the pretreatment, the specimens with their intact scales were subsequently mounted in the HVR to be attacked by the corrosive TAN 3.5 solution. This step was named as "challenge" because specimens were exposed to a much more corrosive condition than that in the pretreatment and the scale formed in the pretreatment was subjected to the attack by the corrosive TAN 3.5 solution as described below.

In the challenge, the HVR was fed with the corrosive TAN 3.5 solution at a flow rate of 7.5 cm^3/min for 24 h at 343° C while rings were rotated at 2000 rpm (equivalent to a peripheral velocity of 8.5 m/s, Reynolds number of 1771 and wall shear stress of 74 Pa). A back-pressure of 1.1×10^6 Pa was maintained on the effluent of the HVR to suppress breakout of gas. In the end of the challenge, the feed of the HVR was switched to the mineral oil, cooled, and the rings removed from the HVR.

Table 1
Chemical composition of A106 carbon steel (CS) specimen (%wt).

C	Si	Mn	P	S	Cr	Ni	Mo	V	Cu	Fe
0.18	0.41	0.8	0.11	0.06	0.02	0.04	0.02	0.03	0.08	Bal

Table 2
Model acids in the preparation of experiment solutions.

Structure of model acid	Pretreatment solution with model acid	Acid boiling point
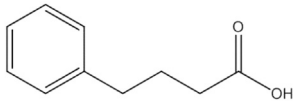	PBA + mineral oil	340 °C
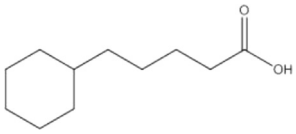	CxPA + mineral oil	331 °C
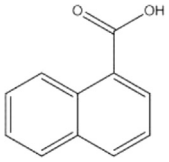	NA + mineral oil	300 °C

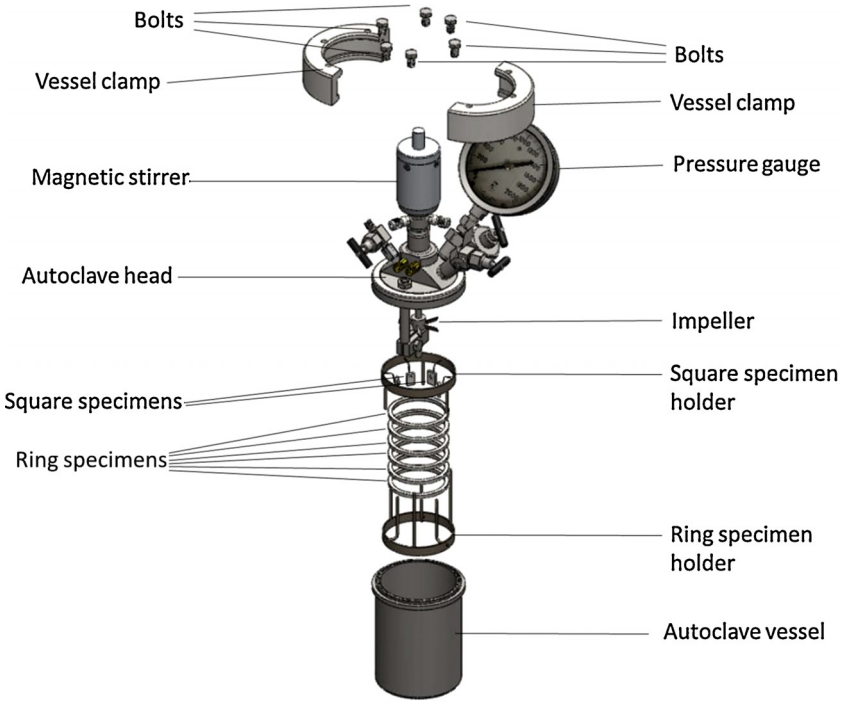

Fig. 1. Exploded view of the stirred autoclave.

Scanning Electron Microscope (SEM) analyses were performed on JEOL JSM-6390 SEM. Some rings were selected to be analyzed by Transmission Electron Microscope (TEM). Sections were cut from the scale with a FEI Helios Nanolab 650 for Focused Ion Beam (FIB) and imaged with a Zeiss Libra 200EF TEM. Both SEM and TEM were combined with Energy Dispersive X-ray Spectroscope (EDS) to analyze the chemical composition. The crystal structure was revealed by X-Ray Diffraction (XRD) analysis performed on Bruker Discover D8 with a Co K-alpha X-ray tube.

2.5. Evaluation of corrosion rates

Corrosion rates of rings were calculated based on their weight loss during the experiment. For the pretreatment experiment conducted in the autoclave, the corrosion rate was calculated using Eq. (8). In the challenge step, freshly abraded rings were pretreated in the autoclave followed by the challenge in the HVR. The challenge corrosion rate was assessed by Eq. (9).

$$V_1 = \frac{87600\Delta W_1}{\rho A_1 t} \tag{8}$$

$$V_2 = \frac{87600(\Delta W_2 - \Delta W_1)}{\rho A_2 t} \tag{9}$$

In Eqs. (8) & (9), V_1 is the pretreatment corrosion rate, mm/y; V_2 is the challenge corrosion rate, mm/y; 87600 is the unit conversion constant; ΔW_1 is the weight loss in the pretreatment step, g; ΔW_2 is the weight loss in the challenge step, g; ρ is the density of ring specimen, g/cm^3; A_1 is the area of ring specimen exposed to pretreatment solution during the pretreatment, cm^2; A_2 is the area of ring specimen exposed to corrosive TAN 3.5 solution during challenge, cm^2; t is the corrosion time, h.

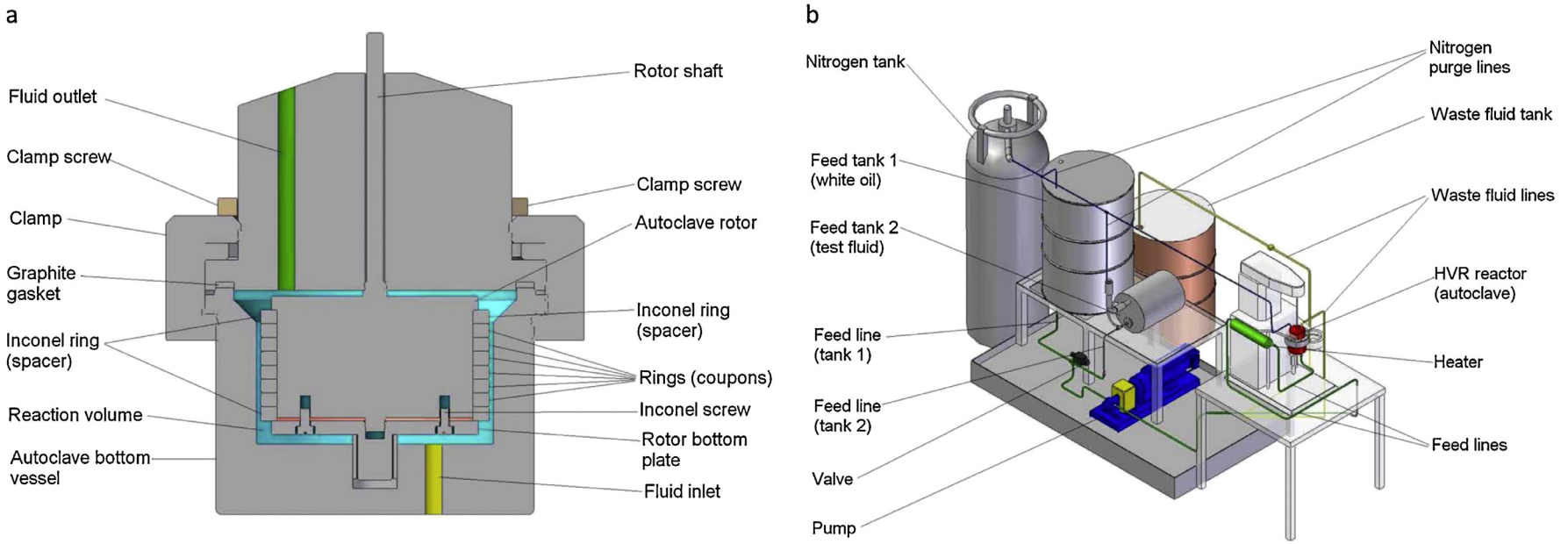

Fig. 2. Cross-section view of High Velocity Rig (HVR) reactor (a) and scheme of HVR (b).

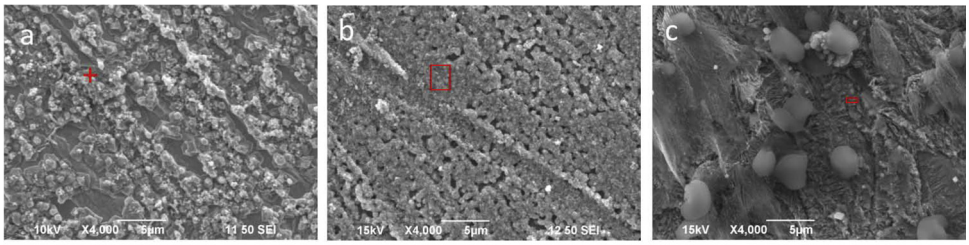

Element	At%
C	21.24
O	51.44
Fe	58.59

Element	At%
C	11.22
O	15.61
Fe	73.17

Element	At%
C	20.99
Fe	79.01

Fig. 3. Plain-view SEM and EDS analysis of rings pretreated in "PBA + mineral oil" (a), "CxPA + mineral oil" (b), and "NA + mineral oil" (c) at 316° C. The EDS analysis was performed in the red areas shown in the SEM images and contains all detected elements. (For interpretation of the references to colour in this figure legend, the reader is referred to the web version of this article.)

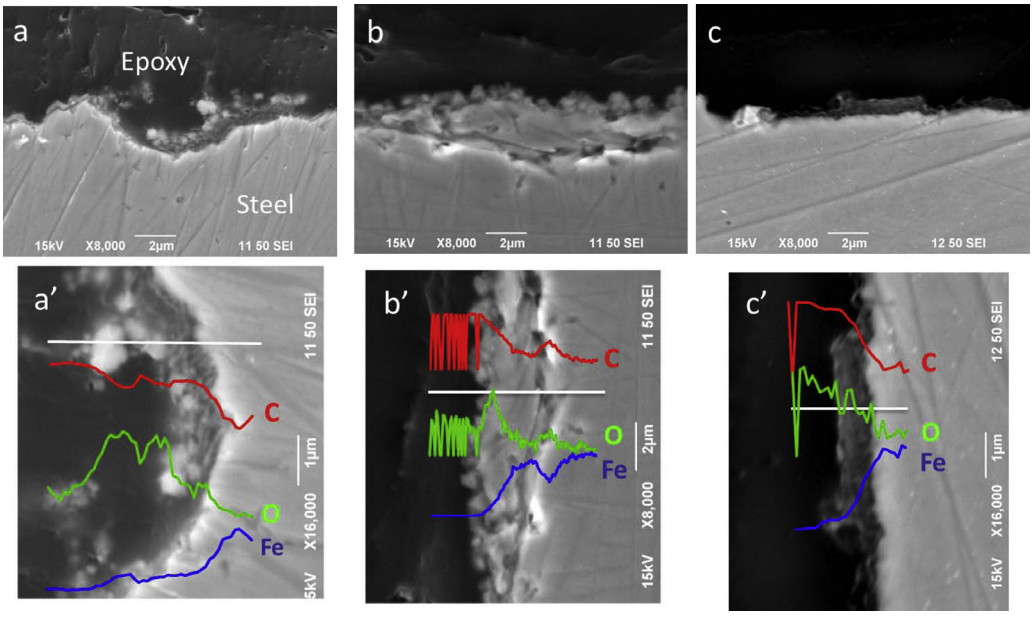

Fig. 4. Cross-section SEM analysis of rings pretreated in "PBA + mineral oil" (a), "CxPA + mineral oil" (b), and "NA + mineral oil" (c) at 316° C. The EDS analysis showing atomic percent of element was performed along the white line in images a′, b′, and c′.

Table 3
Pretreatment and challenge corrosion rates of rings pretreated in "PBA + mineral oil", "CxPA + mineral oil", and "NA + mineral oil" at 316° C.

Pretreatment Solution	Pretreatment Corrosion Rate (mm/y)	Challenge Corrosion Rate (mm/y)
PBA + mineral oil	0.3	3.8
CxPA + mineral oil	0.3	7.4
NA + mineral oil	0.6	5.8
Pure TAN 3.5 corrosion rate	–	7.8

3. Results

3.1. Effect of acid structure on corrosion rates

Corrosion rates for CS rings pretreated at 316° C in PBA, CxPA, and NA at TAN 1.75 are shown in Table 3. Although the pretreatment corrosion rates were low, the NA corrosion rate was twice that of the other two model acids. Pretreatment with CxPA and NA lowered the challenge corrosion rates below the pure TAN 3.5 corrosion rate to some extent. Pure TAN 3.5 corrosion rate refers to the HVR challenge corrosion rate of freshly abraded rings (without pretreatment) by the corrosive TAN 3.5 solution at 343° C. On the other hand, pretreatment in PBA appears the most effective in reducing corrosion in the challenge, suggesting that protective scale formation may have occurred.

3.2. Effect of temperature on PBA corrosion rates

Among three model acids, pretreatment in PBA was the most effective to form the protective scale. To determine if lowering the pretreatment temperature affected the oxide scale formation, rings were pretreated in "PBA + mineral oil" at 288° C and then challenged as before. The scale formed with PBA at 288 ° C was thinner and more granular than the one formed at 316° C (see the TEM analysis below). However, corrosion rates were very similar to those for the 316° C PBA pretreatment (Table 4). Thus, the lower temperature did not affect the marginal protectiveness of the oxide scale generated by the PBA.

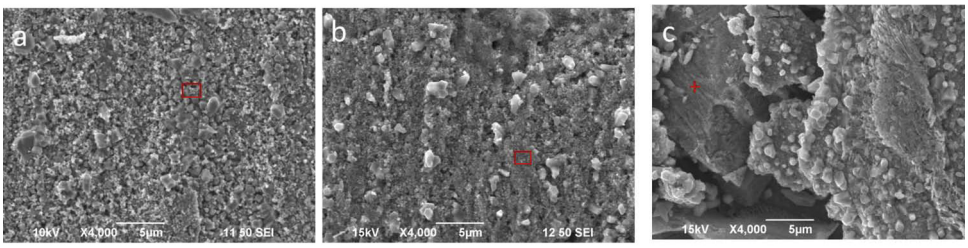

Element	At%
C	24.05
O	47.26
S	9.75
Fe	18.94

Element	At%
C	13.30
O	21.03
S	17.98
Fe	47.69

Element	At%
C	8.98
O	6.11
S	3.77
Fe	81.14

Fig. 5. Surface SEM and EDS analysis of rings pretreated in "PBA + mineral oil" (a), "CxPA + mineral oil" (b), and "NA + mineral oil" (c) after the challenge. The EDS analysis was performed in the red areas shown in the SEM images and contains all detected elements. (For interpretation of the references to colour in this figure legend, the reader is referred to the web version of this article.)

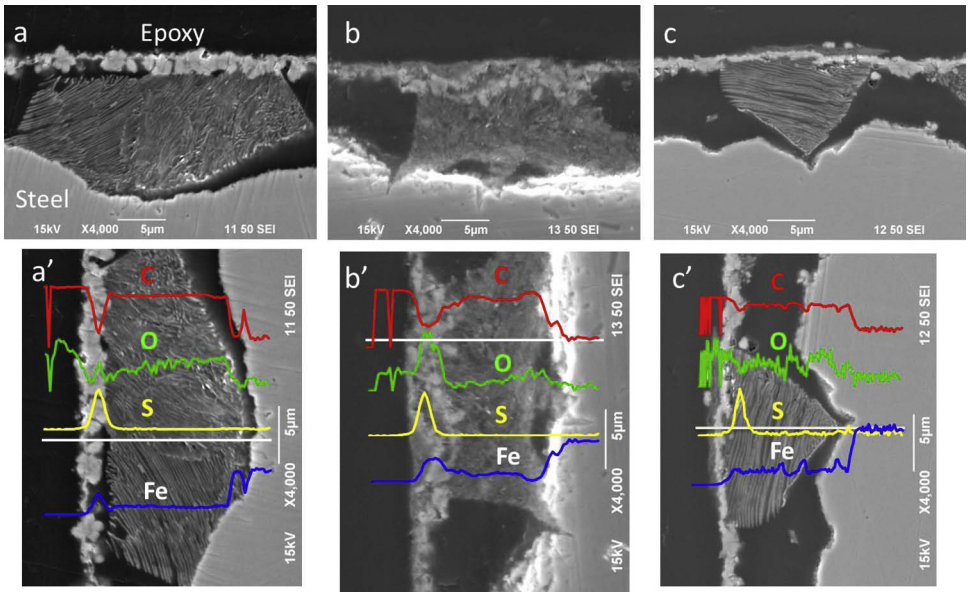

Fig. 6. Cross-section SEM analysis of rings pretreated in "PBA + mineral oil" (a), "CxPA + mineral oil" (b), and "NA + mineral oil" (c) at 316° C after the challenge by the corrosive TAN 3.5 solution at 343 ° C. The EDS analysis showing atomic percent of element was performed along the white line in images a′, b′, and c′.

Table 4
Pretreatment and challenge corrosion rates of rings pretreated in "PBA + mineral oil" at 288° C.

Pretreatment Solution	Pretreatment Corrosion Rate (mm/y)	Challenge Corrosion Rate (mm/y)
PBA + mineral oil	0.4	4.6
Pure TAN 3.5 corrosion rate	–	7.8

3.3. SEM analysis of corrosion product scales

Plain-view SEM/EDS analyses of the CS rings pretreated in pretreatment solutions are shown in Fig. 3. A continuous scale is observed on the ring surface pretreated in PBA (image a) or CxPA (image b). Although spot EDS analysis (indicated in red) reveals that both scales are composed of iron and oxygen, the PBA scale exhibits a much higher level of oxygen. The pretreatment in NA, on the other hand, resulted in a surface with isolated particles rather than a continuous scale (image c). In the latter, no oxygen is detected in the EDS analysis (in the area indicated) which suggests that the NA did not promote the formation of a continuous oxide scale.

The corresponding cross-section SEM images of scales formed in "PBA + mineral oil" and EDS scanning analysis shows a broad peak of oxygen adjacent to the steel surface (images a and a′ of Fig. 4). The scale formed with CxPA is also quite thin and EDS analysis indicates the presence of oxygen (images b and b′ of Fig. 4). Cross-section SEM image of the steel pretreated in NA (image c of Fig. 4) reveals an isolated area composed of iron and oxide rather than a continuous scale, which is consistent with the findings of plain-view SEM/EDS analysis. It suggests that NA did not effectively promote the formation of a robust oxide scale.

Challenge corrosion rates for all three acid pretreatments are higher than 3 mm/y, but less than the pure TAN 3.5 corrosion rate (Table 3). Plain-view SEM analysis of rings after the challenge shows that the scale in all three cases has picked up a minor amount of sulfur (Fig. 5).The presence of sulfur in the scales after the challenge can be attributed to trace sulfur content in the TCI, as previously

reported [30]. In contrast to the coherent scale on rings pretreated with for PBA and CxPA, the rings pretreated with NA exhibit a broken, delaminated scale with predominantly iron exposed at the EDS spot. EDS analyses of the PBA and CxPA pretreated rings show that some oxygen remains on the surface.

The corresponding cross-section SEM analyses show that detached scales are formed on rings for all three acid pretreatments after the challenge (Fig. 6). In all three cases, cross-section EDS analyses were performed across pearlite grains showing sulfur (from TCI) and carbon (from the cementite in the pearlite), but oxygen content is minimal. These results suggest that acid in the corrosive TAN 3.5 solution has dissolved (or diffused through) the thin oxide scales formed in the pretreatment (seen in Fig. 4) and corroded the underneath ferritic iron in the steel leaving pillars of pearlite under the sulfide layer. Differences in corrosion resistance among acids are consistent with the integrity of the oxide scale formed in the pretreatment. For PBA, the oxide scale reduces corrosion rates while the porous oxides from CxPA and fragmented oxides from NA offer little resistance.

In summary, PBA is most effective among the three selected model acids in the formation of oxide scale that deters the NAP corrosion while CxPA and NA are less effective. The resolution of SEM images is not high enough to reveal the structure of the oxides on the surface. It is not clear from the SEM analysis whether the thin oxide scale produced in the pretreatments were reducing corrosion throughout the challenge or that the oxide scale temporarily retarded corrosion until it was destroyed.

3.4. TEM analysis of scale formed in PBA

To evaluate the effect of oxide scales, high-resolution TEM and XRD analyses were performed on both pretreated and challenged rings in the "PBA + mineral oil" experiment. The TEM image of the ring pretreated in PBA reveals a thin scale (Fig. 7). EDS mapping confirms that the scale is composed of oxygen and iron (Fig. 8). The TEM image and its corresponding EDS mapping analysis also show that there are some white areas in the scale which are deficit in oxygen but rich in carbon. This is consistent with small fragments

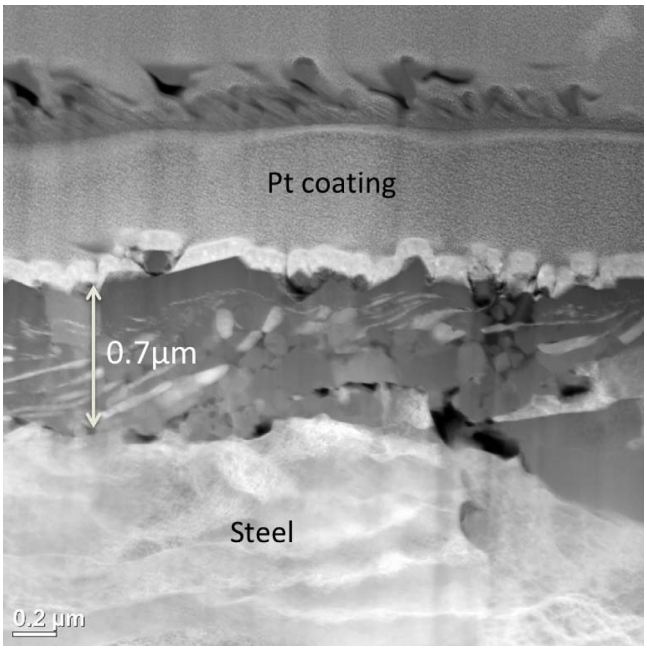

Fig. 7. TEM image of the scale on the ring pretreated in "PBA + mineral oil" at 316° C.

of cementite (Fe_3C) that are not corroded by PBA. The EDS line scanning (Fig. 9) shows that the oxygen accounts to about 60% in the scale, which is consistent with the finding of magnetite in the XRD analysis (Fig. 10).

The scale formed in PBA pretreatment at 288 ° C shows a thinner layer of larger particles with gaps between them (Fig. 11). EDS mapping (Fig. 12) demonstrates that the scale is composed of iron oxide, possibly with some cementite buried within, as suggested by the EDS line scanning (Fig. 13).

TEM shows that most of the oxide scale from the PBA pretreatment at 316 ° C is removed by the corrosive TAN 3.5 solution (Fig. 14). EDS mapping only detects isolated oxide particles (Fig. 15)

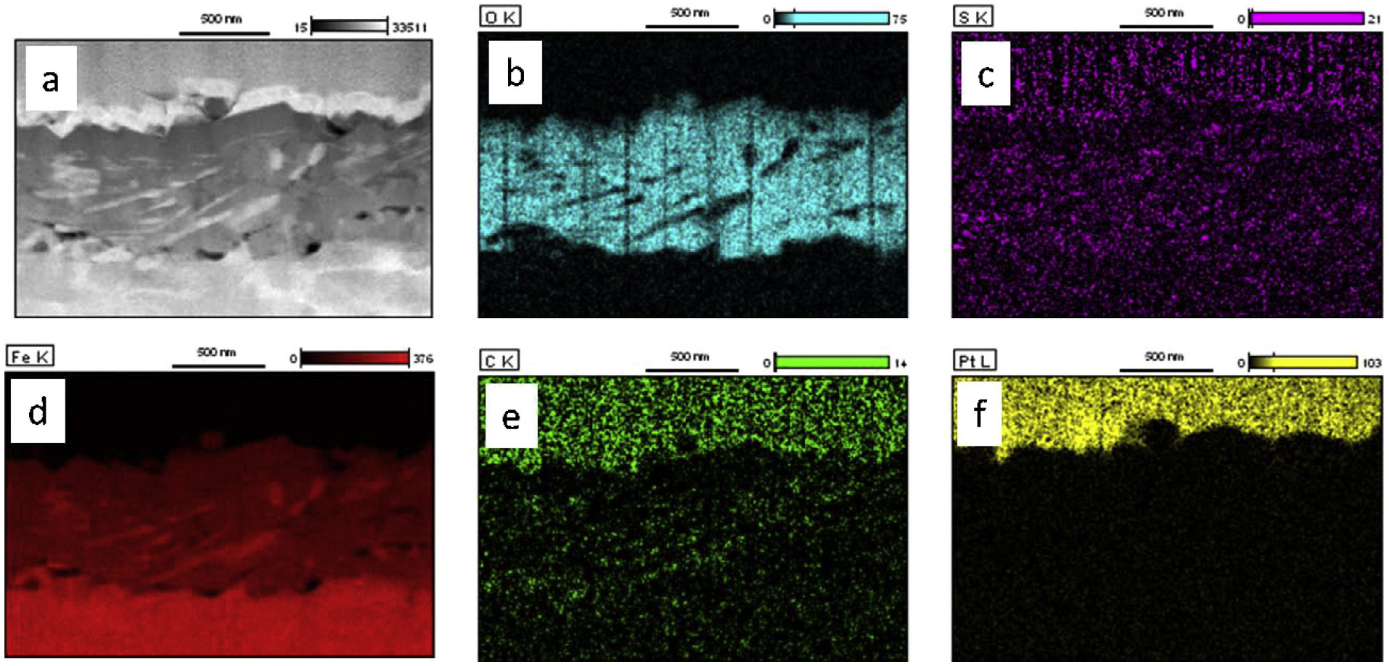

Fig. 8. EDS mapping of the scale on the ring pretreated in "PBA + mineral oil" at 316° C, showing the TEM image (a) and elemental distribution of O (b), S (c), Fe (d), C (e), and Pt (f).

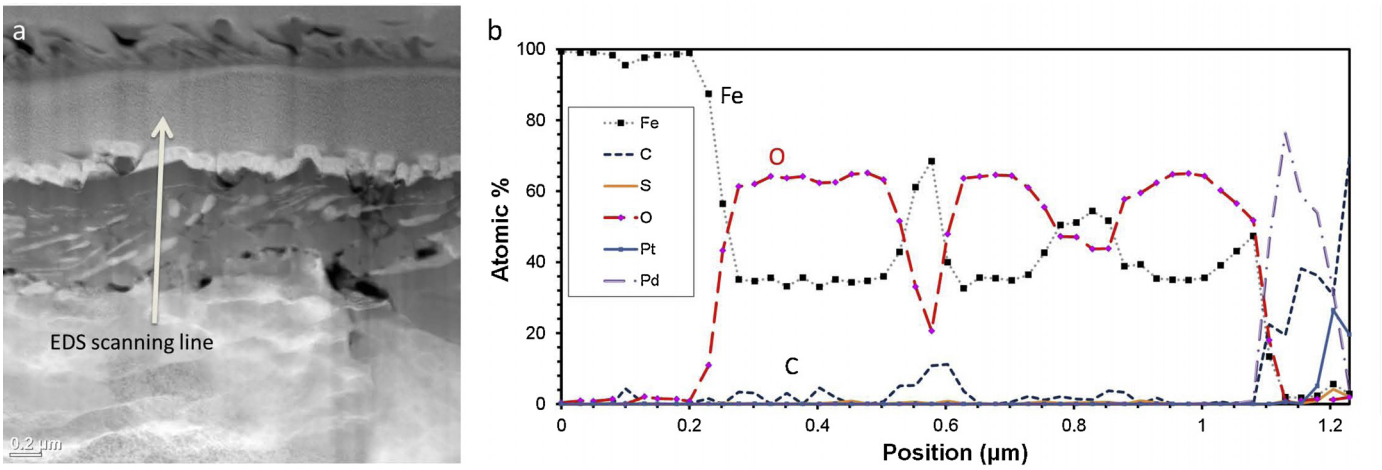

Fig. 9. Elemental profile of the scale on the ring pretreated in "PBA + mineral oil" at 316° C. (a) Image of the scale with the line of EDS scanning; (b) Results of EDS analysis showing atomic percent of element.

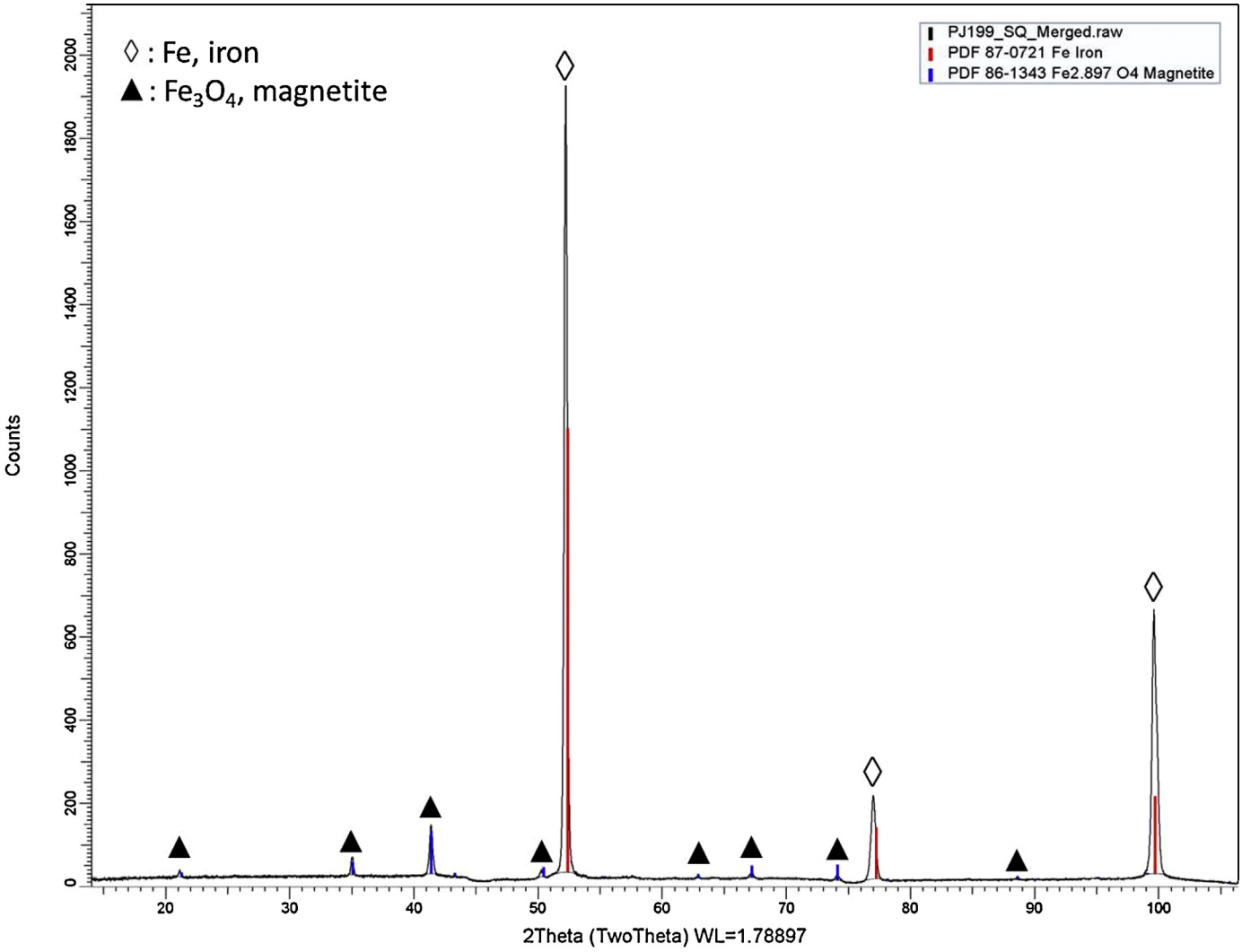

Fig. 10. XRD pattern of the scale on the ring pretreated in "PBA + mineral oil" at 316° C (TEM image shown in Fig. 7 and elemental profile shown in Fig. 8 and Fig. 9).

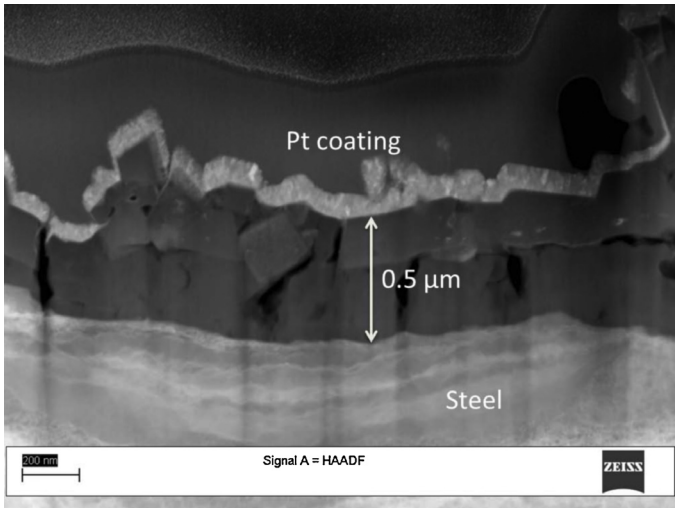

Fig. 11. TEM image of the scale on the ring pretreated in "PBA + mineral oil" at 288° C.

that XRD analysis identifies as magnetite (Fe_3O_4) (Fig. 16). The troilite, seen in the XRD, is a form of pyrrhotite (FeS) that may be formed due to the sulfur content in the corrosive TAN 3.5 solution as mentioned above.

4. Discussion

4.1. NAP as source of oxygen in magnetite scale

Prior to our recent research, NAP corrosion was generally considered to generate soluble iron naphthenates only, i.e., to leave no solid corrosion product on the steel surface. However, oxides had been reported in the NAP corrosion literature. Oxides had been detected by X-ray Photoelectron Spectroscope (XPS) analysis on scales after autoclave experiments with crude fractions [44]. Magnetite had been detected in plane XRD analyses of scales from a high-TAN crude [45] and from commercial NAP [46]. However, the oxygen in these findings had been dismissed as sample contamination or experimental artifact.

The pretreatment results confirm the hypothesis that acids are the source of oxygen in the magnetite. Previously, we reported that the pretreatment with a solution containing both TCI and a sulfur compound resulted in an oxide scale adjacent to the steel surface and an iron sulfide scale on the top [29]. The location of oxide scales under the sulfide argues against oxidation of iron sulfide scale by air exposure after the pretreatment. When the pretreatment was done at lower temperature (232° C) where corrosion was minimal, no oxide scale was formed by the TCI demonstrating that it was only formed at the higher temperature where corrosion occurred [34]. Although mixed Fe_3O_4 and $Fe(OH)_2$ layers form when iron surfaces are exposed for an hour to 70% relative humidity at ambient temperature, these layers are ~1 nm thick [47]. Thus, the thicker oxide scales (>500 nm) detected in the TEM analysis were formed during the pretreatment. To eliminate dissolved oxygen as a source of the oxide scale, rings were pretreated in the mineral oil (without NAP or any other component) at 316° C. The rings were not corroded (the corrosion rate was zero), abrading marks are still visible, and no oxygen was detected in the EDS analysis (Fig. 17). In sum, our experiments demonstrate that NAP is the sole source of the oxygen in magnetite in the protocol experiments.

4.2. Mechanism of magnetite formation in NAP corrosion

As discussed in the Introduction, wüstite (FeO) can be formed by thermal ketonization of iron naphthenates in solution at temperatures higher than 250° C (Eq. (4)). Previously, we proposed that magnetite is formed below sulfide scale by ketonization during corrosion. We hypothesized that ketonization was faster than iron naphthenate desorption and diffusion through the sulfide layer into the bulk liquid. Here we report that the magnetite can be formed in the pretreatment with model acids in the absence of sulfur compounds. Thus, the model acids study shows that corrosion at 316° C in mineral oil not only forms soluble iron carboxylates but also

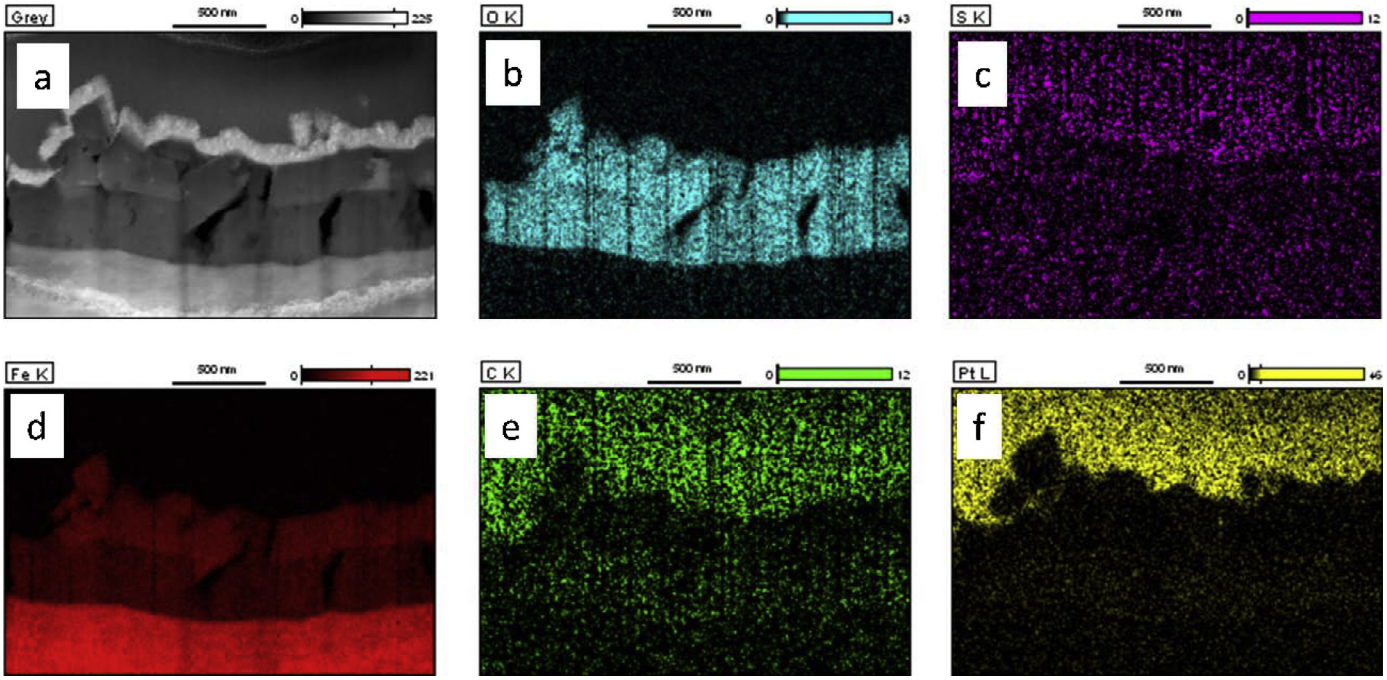

Fig. 12. EDS mapping of the scale on the ring pretreated in "PBA + mineral oil" at 288° C, showing the TEM image (a) and elemental distribution of O (b), S (c), Fe (d), C (e), and Pt (f).

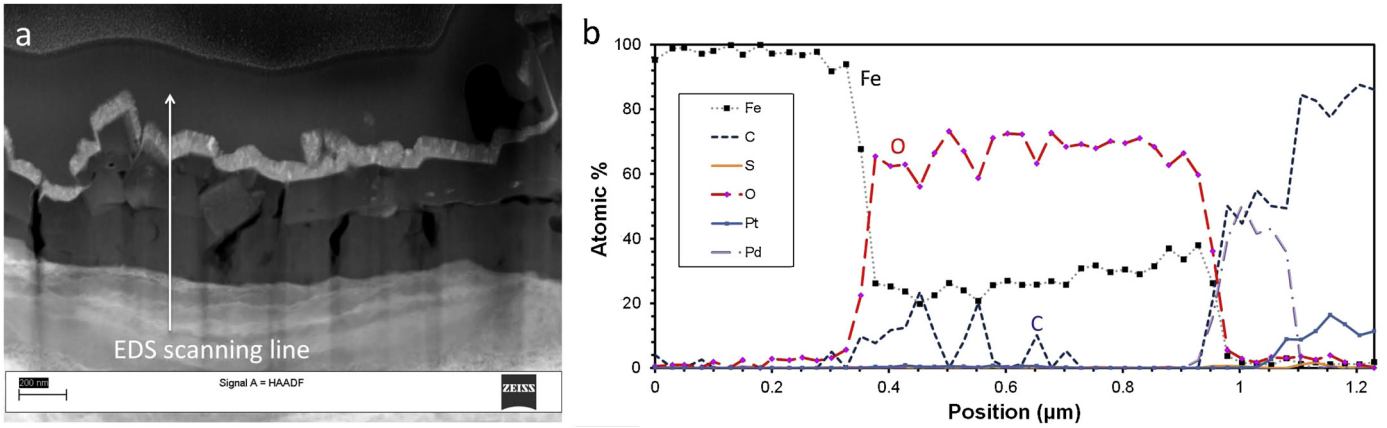

Fig. 13. Elemental profile of the scale on the ring pretreated in "PBA + mineral oil" at 288° C. (a) Image of the scale with the line of EDS scanning; (b) Results of EDS analysis showing atomic percent of element.

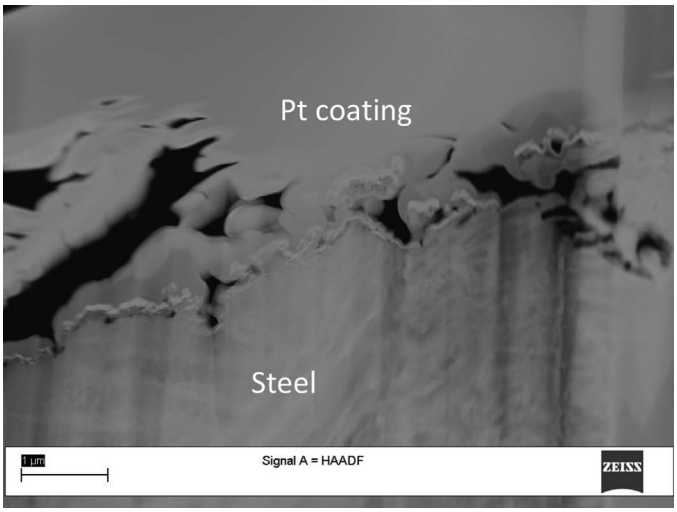

Fig. 14. TEM image of the scale on the ring pretreated in "PBA + mineral oil" at 316° C after the challenge by the corrosive TAN 3.5 solution at 343° C.

leaves a magnetite layer on carbon steel. Because the existence of a magnetite layer in NAP corrosion has only recently been recognized, the conversion of wüstite to magnetite has received little attention in corrosion studies.

However, in recent years, the thermal decomposition of iron carboxylates has been studied extensively as a method for producing mono-disperse nanoparticulate iron oxides with diameters ranging from 5 to 100 nm [26,48]. A majority of these methods prepare iron carboxylates from iron (III) salts before thermal degradation at higher temperature in the presence of excess high molecular weight carboxylic acids (especially oleic acid) in high boiling hydrocarbon solvents. Although wüstite is the primary product of the reaction, the isolated nanoparticulates may be hematite (α-Fe_2O_3), maghemite (γ-Fe_2O_3), and magnetite (Fe_3O_4) depending on the temperature and oxidation conditions employed [48]. However, wüstite apparently plays a similar role in cases where iron (II) salts or iron powder and carboxylic acids are involved [23–25]. Wüstite has a crystal structure with Fe and O forming nonstoichiometric Fe_xO (x = 0.83-0.96) and Fe vacancies in an ordered distribution [49,50]. The structure is not chemically stable and is

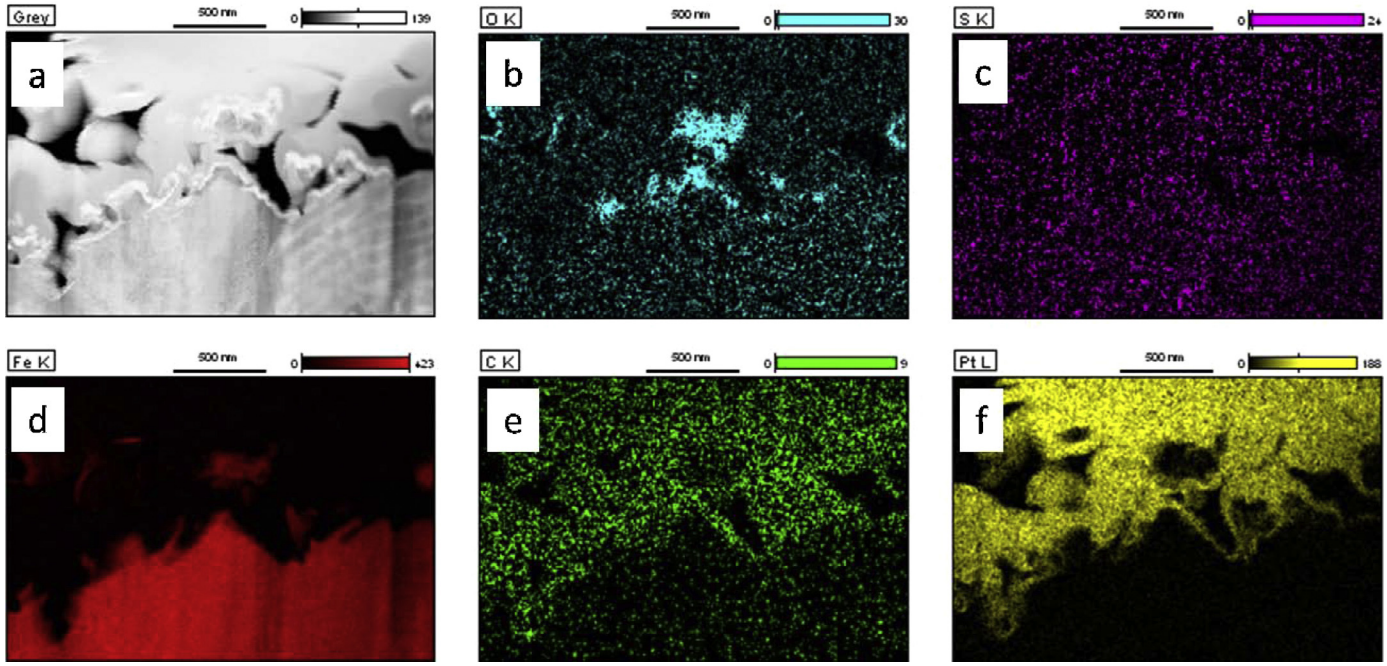

Fig. 15. EDS mapping of the scale on the ring pretreated in "PBA + mineral oil" at 316° C after the challenge by the corrosive TAN 3.5 solution at 343° C, showing the TEM image (a) and elemental distribution of O (b), S (c), Fe (d), C (e), and Pt (f).

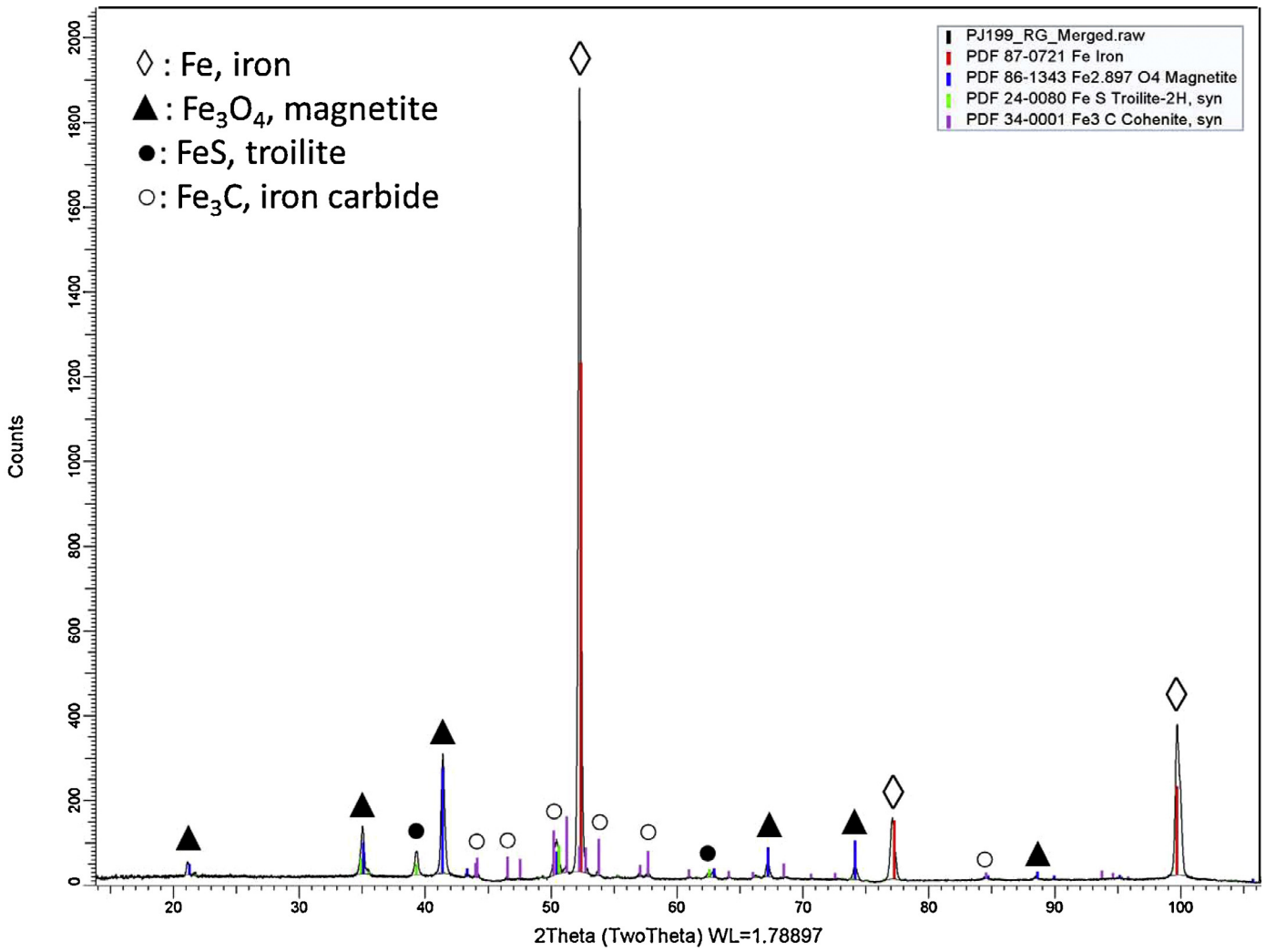

Fig. 16. XRD pattern of the scale on the ring pretreated in "PBA + mineral oil" at 316° C after the challenge by the corrosive TAN 3.5 solution at 343° C (TEM image shown in Fig. 14 and elemental profile shown in Fig. 15).

prone to decomposition into α-Fe and inverse spinel Fe_3O_4 or to oxidation to form γ-Fe_2O_3. This chemical reactivity makes isolation of wüstite nanoparticles difficult; rather, wüstite was converted to one of the other more stable iron oxide forms [23,26,27,51,52]. Oxidation conditions favor maghemite and ultimately hematite; reducing conditions favor magnetite [23,26,27,51,52]. The magnetic properties and size distribution appear to be a function of the acid size/structure, temperature, the solvent, and the acid/iron ratio [24,27,51]. With fatty acids, the excess acids solubilize the iron precursor and stabilize the iron oxide nanoparticles formed during thermal decarboxylation [25,52]. The excess acids also affect the nucleation and aggregation of molecular wüstite into nanoparticulates of different sizes [53–55].

Spent pretreatment solutions were analyzed by positive Electrospray Ionization Fourier Transform Ion Cyclotron Resonance Mass Spectrometry. The formation of ketones consistent with Eq. (4) was found for PBA and CxPA, but not for NA. That is, the spent PBA pretreatment solution for contained 1,7-diphenyl-4-heptanone ($C_{19}H_{22}O$) (Fig. 18) (More detailed results will be reported in a separate publication). Ketonization of iron carboxylates has been proposed to proceed by either a concerted rearrangement involving a ketene intermediate or by a free radical cleavage mechanism [21,56,57]. In either case, the reaction requires α-H on the carbon adjacent to the carboxyl group, i.e. =CH—COOH. Because no α-H is available on aromatic acids, iron salts of aromatic acids cannot form ketones. The failure of NA pretreatment to provide corrosion resistance reflects its inability to ketonize. On the other hand, reaction of iron powder with mixtures or aromatic and aliphatic acids form ketones rapidly because one of the acids has an α-H [19,25].

However, the magnetite detected on the pretreated surfaces surface are not nanoparticulate, but rather much larger. Similar results were noted in the iron powder study, i.e., carboxylic acids without long aliphatic chains were noted to form larger agglomerated magnetite particles [25]. This may be attributed to a less effective adsorption layer of unreacted acids in contrast to "shell" observed in the thermolysis of large fatty acid iron salts [22,52,53,56].

6. Conclusions

The pretreatment at 316° C with model acids produces thin weakly adherent oxide scales on CS rings, i.e. not all naphthenic acid corrosion products leave the metal surface. SEM analyses reveal that the PBA pretreatment produced a compact continuous oxide scale whereas the CxPA scale is less compact and the NA left only discrete particles. Detection of acid-derived ketones in spent pre-

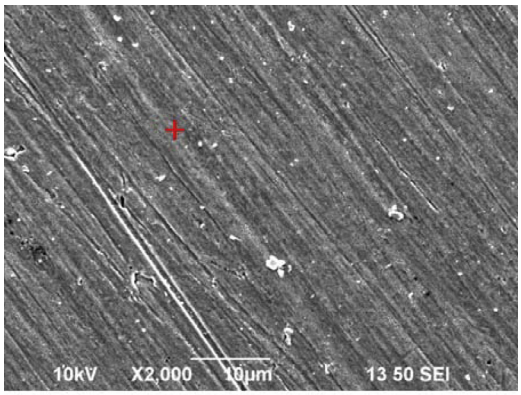

Element	At%
C	6.1
Fe	93.9

Fig. 17. Plain-view SEM and EDS analysis of rings pretreated in the mineral oil at 316° C. The EDS analysis was performed in the red area shown in the SEM image and contains all detected elements. (For interpretation of the references to colour in this figure legend, the reader is referred to the web version of this article.)

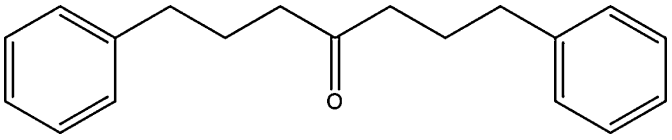

Fig. 18. Ketone identified in spent PBA pretreatment solution at 316° C: 1,7-diphenyl-4-heptanone ($C_{19}H_{22}O$).

treatment PBA and CxPA solutions supports thermal decomposition of iron carboxylates as a source of iron oxides while other oxygen sources have been ruled out. NA appears to be more corrosive (dissolved more iron) but did not yield much iron oxide because it cannot decompose by the same mechanism. The compact PBA oxide scale was the most resistant to the higher severity (TAN 3.5/343° C) challenge in the flow-through HVR. TEM and XRD identified the PBA-derived oxide to be magnetite. Particles of magnetite were formed by structural rearrangement of the wüstite produced initially in the ketonization reaction. The magnetite formed in pretreatment appears to have agglomerated to larger sizes than the nano-particulate ferrites produced by the thermal decarboxylation of large fatty acid iron salts. SEM and TEM examination of the scales before and after the challenge reveals that the magnetite was mostly destroyed during the challenge. At the end of the challenge, the surface is covered by a thin sulfide layer (from the corrosive TAN 3.5 solution) supported on residual pearlitic structures. Differences among the acid "protection" might be attributed to the time required for the acid to break down magnetite scales.

Acknowledgements

This work was supported by Naphthenic Acid Corrosion Joint Industry Project (NAP JIP) in the Institute for Corrosion and Multiphase Technology, Ohio University.

Ketone analyses were carried out by Logan Krajewski at the National High Field Magnet Lab (NHFML) at Florida State University (FSU) using positive Electrospray Ionization Fourier Transform Ion Cyclotron Resonance Mass Spectrometry [(+) ESI/FT/ICR/MS].

References

[1] E. Slavcheva, B. Shone, A. Turnbull, Review of naphthenic acid corrosion in oil refining, Br. Corros. J. 34 (1999) 125–131.
[2] H.L. Craig Jr., Temperature and velocity effects in naphthenic acid corrosion, Corrosion/1996, Paper No. 603, NACE, Houston, TX, USA, (1996).
[3] D.R. Qu, Y.G. Zheng, H.M. Jing, Z.M. Yao, W. Ke, High temperature naphthenic acid corrosion and sulphidic corrosion of Q235 and 5Cr1/2Mo steels in synthetic refining media, Corros. Sci. 48 (2006) 1960–1985.
[4] X.Q. Wu, H.M. Jing, Y.G. Zheng, Z.M. Yao, W. Ke, Resistance of Mo-bearing stainless steels and Mo-bearing stainless-steel coating to naphthenic acid corrosion and erosion–corrosion, Corros. Sci. 46 (2004) 1013–1032.
[5] B.N. Patrick, R. Chakravarti, T.M. Devine, Dynamic measurements of corrosion rates at high temperatures in high electrical resistivity media, Corros. Sci. 94 (2015) 99–103.
[6] E. Babaian-Kibala, H.L. Craig Jr., G.L. Rusk, K.V. Blanchard, T.J. Rose, B.L. Uehlein, R.C. Quinter, M.A. Summers, Naphthenic acid corrosion in refinery settings, Mater. Perform. 32 (1993) 50–55.
[7] R.B. Rebak, Sulfidic corrosion in refineries–a review, Corros. Rev. 29 (2011) 123–133.
[8] R.D. Kane, B. Chambers, High temperature crude oil corrosivity: where sulfur and naphthenic acid chemistry and metallurgy meet, in: Corrosion Solutions Conference, Lake Louise, Alberta, Canada, 2011.
[9] A.E. Turnbull, E. Slavcheva, B. Shone, Factors controlling naphthenic acid corrosion, Corrosion 54 (1998) 922–930.
[10] S.D. Kapusta, A. Ooms, A. Smith, F. van den Berg, W. Fort, Safe processing of acid crudes, Corrosion/2004, Paper No. 4637, NACE, Houston, TX, (2004).
[11] B. Messer, B. Tarleton, M. Beaton, T. Phillips, New theory for naphthenic acid corrosivity of athabasca oilsands crudes, Corrosion/2004, Paper No. 4634, NACE, Houston, TX, USA, (2004).
[12] A. Groysman, N. Brodsky, J. Penner, A. Goldis, N. Savchenko, Corrosiveness of acidic crude oil and its fractions, Mater. Perfom. 44 (2005) 34–39.
[13] H.D. Dettman, N. Li, J. Luo, Refinery corrosion, organic acid structure, and Athabasca bitumen, Corrosion/2009, Paper No. 9336, NACE, Houston, TX, USA, (2009).
[14] O. Yepez, Influence of different sulfur compounds on corrosion due to naphthenic acid, Fuel 84 (2005) 97–104.
[15] J. Hau, Predicting sulfidic and naphthenic acid corrosion, Corrosion 65 (2009) 831–844.
[16] O. Yepez, On the chemical reaction between carboxylic acids and iron, including the special case of naphthenic acid, Fuel 86 (2007) 1162–1168.
[17] D.F. Smith, R.P. Rodgers, P. Rahimi, A. Teclemariam, A.G. Marshall, Effect of thermal treatment on acidic organic species from Athabasca bitumen heavy vacuum gas oil, analyzed by negative-ion electrospray Fourier transform ion cyclotron resonance (FT-ICR) mass spectrometry, Energy Fuels 23 (2008) 314–319.
[18] R. Davis, H.P. Schultz, Studies of thermal decarboxylation of iron carboxylates. I. preparation of symmetrical aliphatic ketones, JOC 27 (1962) 854–857.
[19] C. Granito, H.P. Schultz, Decarboxylation studies. II. preparation of alkyl phenyl ketones, JOC 28 (1963) 879–881.
[20] M. Renz, Ketonization of carboxylic acids by decarboxylation: mechanism and scope, Eur. J. Org. Chem. 2005 (2005) 979–988.
[21] L.J. Goossen, P. Mamone, C. Oppel, Catalytic decarboxylative cross–ketonisation of aryl–and alkylcarboxylic acids using magnetite nanoparticles, Adv. Synth. Catal. 353 (2011) 57–63.
[22] G. Kataby, M. Cojocaru, R. Prozorov, A. Gedanken, Coating carboxylic acids on amorphous iron nanoparticles, Langmuir 15 (1999) 1703–1708.
[23] C.J. Chen, H.Y. Lai, C.C. Lin, J.S. Wang, R.K. Chiang, Preparation of monodisperse iron oxide nanoparticles via the synthesis and decomposition of iron fatty acid complexes, Nanoscale Res. Lett. 4 (2009) 1343–1350.
[24] N.R. Jana, Y. Chen, X. Peng, Size-and shape-controlled magnetic (Cr, Mn Fe, Co, Ni) oxide nanocrystals via a simple and general approach, Chem. Mater. 16 (2004) 3931–3935.
[25] K.S. Salih, P. Mamone, G. Dörr, T.O. Bauer, A. Brodyanski, C. Wagner, M. Kopnarski, R.N. Klupp Taylor, S. Demeshko, F. Meyer, V. Schünemann, Facile synthesis of monodisperse maghemite and ferrite nanocrystals from metal powder and octanoic acid, Chem. Mater. 25 (2013) 1430–1435.
[26] C.J. Chen, R.K. Chiang, H.Y. Lai, C.R. Lin, Characterization of monodisperse wüstite nanoparticles following partial oxidation, J. Phys. Chem. C 114 (2010) 4258–4263.
[27] F.X. Redl, C.T. Black, G.C. Papaefthymiou, R.L. Sandstrom, M. Yin, H. Zeng, C.B. Murray, S.P. O'Brien, Magnetic, electronic, and structural characterization of nonstoichiometric iron oxides at the nanoscale, JACS 126 (2004) 14583–14599.
[28] G.M. Bota, D. Qu, S. Nesic, A. Wolf, Naphthenic acid corrosion of mild steel in the presence of sulfide scales formed in crude oil fractions at high temperature, Corrosion/2010, Paper No. 10353, NACE, Houston, TX, USA, (2010).
[29] P. Jin, Mechanism of corrosion by naphthenic acids and organosulfur compounds at high temperatures, Ph.D. Dissertation, 2013, Ohio University.

[30] P. Jin, S. Nesic, H.A. Wolf, Analysis of corrosion scales formed on steel at high temperatures in hydrocarbons containing model naphthenic acids and sulfur compounds, Surf. Interface Anal. 47 (2015) 454–465.
[31] H.A. Wolf, F. Cao, S.C. Blum, A.M. Schilowitz, S. Ling, J.E. McLAUGHLIN, S. Nesic, P. Jin, B. Gheorghe, Method for identifying layers providing corrosion protection in crude oil fractions, U.S. Patent 9140640, (2015).
[32] M.M. Barney, T.Z. Miao, M.T. Cheng, G.J. Kusinski, Methods for evaluating corrosivity of crude oil feedstocks, U.S. Patent 8956874, (2015).
[33] G.M. Bota, Corrosion of Steel at High Temperature in Naphthenic Acid and Sulfur Containing Crude Oil Fractions, Ph.D. Dissertation, (2010), Ohio University.
[34] P. Jin, W. Robbins, G. Bota, S. Nesic, Characterization of iron oxide scale formed in naphthenic acid corrosion, in: D. Firrao, M. Zhang, Z. Peng, J.P. Escobedo-Diaz, C. Bai (Eds.), Characterization of Minerals, Metals, and Materials, Wiley, Tennessee, 2016, pp. 115–125, 2016.
[35] G. Bota, F. Farelas, W. Robbins, S. Nesic, Evaluation of scales' protective properties in naphthenic acid challenges, ABSTRACTS OF PAPERS OF THE AMERICAN CHEMICAL SOCIETY 2014 Aug 10 (Vol. 248), Washington, DC, AMER CHEMICAL SOC, (2014), 546–547.
[36] C.S. Hsu, G.J. Dechert, W.K. Robbins, E.K. Fukuda, Naphthenic acids in crude oils characterized by mass spectrometry, Energy Fuels 14 (2000) 217–223.
[37] J.S. Clemente, P.M. Fedorak, A review of the occurrence, analyses, toxicity, and biodegradation of naphthenic acids, Chemosphere 60 (2005) 585–600.
[38] W. Meredith, S.J. Kelland, D. Jones, Influence of biodegradation on crude oil acidity and carboxylic acid composition, Org. Geochem. 31 (2000) 1059–1073.
[39] L.M. Wenger, C.L. Davis, G.H. Isaksen, Multiple controls on petroleum biodegradation and impact on oil quality, SPE Annual Technical Conference and Exhibition, Society of Petroleum Engineers (2001).
[40] C.M. Aitken, D. Jones, S. Larter, Anaerobic hydrocarbon biodegradation in deep subsurface oil reservoirs, Nature 431 (2004) 291–294.
[41] I.M. Head, S.R. Larter, N.D. Gray, A. Sherry, J.J. Adams, C.M. Aitken, D.M. Jones, A.K. Rowan, H. Huang, W.F. Röling, Hydrocarbon degradation in petroleum reservoirs, in: K.N. Timmis (Ed.), Handbook of Hydrocarbon and Lipid Microbiology, Springer, Heidelberg, 2016, pp. 3097–3109.
[42] D. Singh, A. Kumar, A fresh look at ASTM G 1–90 solution recommended for cleaning of corrosion products formed on iron and steels, Corrosion 59 (2003) 1029–1036.
[43] G.1 ASTM - 03, Standard practice for preparing, cleaning, and evaluating corrosion test specimens, West Conshohocken, Pennsylvania.
[44] M. El Kamel, A. Galtayries, P. Vermaut, B. Albinet, G. Foulonneau, X. Roumeau, B. Roncin, P. Marcus, Sulfidation kinetics of industrial steels in a refinery crude oil at 300C: reactivity at the nanometer scale, Surf. Interface Anal. 42 (2010) 605–609.
[45] N.R. Smart, A.P. Rance, A.M. Pritchard, Laboratory investigation of naphthenic acid corrosion under flowing conditions, Corrosion/2002, Paper No. 02484, NACE, Houston, TX, (2002).
[46] B.S. Huang, W.F. Yin, D.H. Sang, Z.Y. Jiang, Synergy effect of naphthenic acid corrosion and sulfur corrosion in crude oil distillation unit, Appl. Surf. Sci. 259 (2012) 664–670.
[47] G. Bhargava, I. Gouzman, C.M. Chun, T.A. Ramanarayanan, S.L. Bernasek, Characterization of the native surface thin film on pure polycrystalline iron: a high resolution XPS and TEM study, Appl. Surf. Sci. 253 (2007) 4322–4329.
[48] W.W. Yu, Synthesis of monodisperse iron oxide nanocrystals by thermal decomposition of iron carboxylate salts, Chem. Commun. 20 (2004) 2306–2307.
[49] Y. Hou, Z. Xu, S. Sun, Controlled synthesis and chemical conversions of FeO nanoparticles, Angew. Chem. 119 (2007) 6445–6448.
[50] G.S. Parkinson, Iron oxide surfaces, preprint arXiv:1602.06774, (2016).
[51] R. Chen, M.G. Christiansen, A. Sourakov, A. Mohr, Y. Matsumoto, S. Okada, A. Jasanoff, P.O. Anikeeva, High-performance ferrite nanoparticles through nonaqueous redox phase tuning, Nano Lett. 16 (2016) 1345–1351.
[52] L. Zhang, R. He, H.C. Gu, Oleic acid coating on the monodisperse magnetite nanoparticles, Appl. Surf. Sci. 253 (2006) 2611–2617.
[53] N.T. Thanh, N. Maclean, S. Mahiddine, Mechanisms of nucleation and growth of nanoparticles in solution, Chem. Rev. 114 (2014) 7610–7630.
[54] J. van Embden, A.S. Chesman, J.J. Jasieniak, The heat-up synthesis of colloidal nanocrystals, Chem. Mater. 27 (2015) 2246–2285.
[55] W. Wu, Z. Wu, T. Yu, C. Jiang, W.S. Kim, Recent progress on magnetic iron oxide nanoparticles: synthesis, surface functional strategies and biomedical applications, Sci. Technol. Adv. Mater. 16 (2015) 1–43.
[56] N.J. Turro, P.H. Lakshminarasimhan, S. Jockusch, S.P. O'Brien, S.G. Grancharov, F.X. Redl, Spectroscopic probe of the surface of iron oxide nanocrystals, Nano Lett. 2 (2002) 325–328.
[57] R.A. Hites, K. Biemann, Mechanism of ketonic decarboxylation. Pyrolysis of calcium decanoate, JACS 94 (1972) 5772–5777.
[58] P. Jin, F. Farelas, W. Robbins, G. Bota, S. Nesic, Generation of H2 S by crude fractions at high temperature, In: ABSTRACTS OF PAPERS OF THE AMERICAN CHEMICAL SOCIETY 2014 Aug 10 (Vol. 248), Washington, DC, AMER CHEMICAL SOC, (2014), 544–545.